ELSEVIER

Journal of Biotechnology 92 (2001) 113–131

JOURNAL OF Biotechnology

www.elsevier.com/locate/jbiotec

Tubular photobioreactor design for algal cultures

E. Molina, J. Fernández, F.G. Acién, Y. Chisti *

Department of Chemical Engineering, University of Almería, E-04071 Almeria, Spain

Received 13 June 2000; received in revised form 6 October 2000; accepted 13 October 2000

Abstract

Principles of fluid mechanics, gas–liquid mass transfer, and irradiance controlled algal growth are integrated into a method for designing tubular photobioreactors in which the culture is circulated by an airlift pump. A 0.2 m^3 photobioreactor designed using the proposed approach was proved in continuous outdoor culture of the microalga *Phaeodactylum tricornutum*. The culture performance was assessed under various conditions of irradiance, dilution rates and liquid velocities through the tubular solar collector. A biomass productivity of 1.90 g l^{-1} d^{-1} (or 32 g m^{-2} d^{-1}) could be obtained at a dilution rate of 0.04 h^{-1}. Photoinhibition was observed during hours of peak irradiance; the photosynthetic activity of the cells recovered a few hours later. Linear liquid velocities of 0.50 and 0.35 m s^{-1} in the solar collector gave similar biomass productivities, but the culture collapsed at lower velocities. The effect of dissolved oxygen concentration on productivity was quantified in indoor conditions; dissolved oxygen levels higher or lower than air saturation values reduced productivity. Under outdoor conditions, for given levels of oxygen supersaturation, the productivity decline was greater outdoors than indoors, suggesting that under intense outdoor illumination photooxidation contributed to loss of productivity in comparison with productivity loss due to oxygen inhibition alone. Dissolved oxygen values at the outlet of solar collector tube were up to 400% of air saturation.

Keywords: Photobioreactors; Microalgae; *Phaeodactylum tricornutum*

Nomenclature

A	total land area occupied by reactor tubes (m^2)
A_r	cross-sectional area of riser (m^2)
A_D	perpendicular cross-sectional area of degasser (m^2)
A_d	cross-sectional area of downcomer (m^2)
C	tracer concentration (mol l^{-1})
C_b	biomass concentration (g l^{-1})

* Corresponding author. Present address: Institute of Technology and Engineering, Massey University, Private Bag 11222, Palmerston North, New Zealand.

E-mail address: y.chisti@massey.ac.nz (Y. Chisti).

0168-1656/01/$ - see front matter
PII: S0168-1656(01)00353-4

C_S	concentration of suspended solids (g l^{-1})
D	dilution rate (h^{-1})
d	horizontal spacing between tubes (m)
d_B	mean bubble diameter (m)
d_t	tube diameter (m)
D_L	diffusivity of the transferring gas in liquid (m^2 s^{-1})
f	scale factor
g	gravitational acceleration (m s^{-2})
h	vertical spacing between tubes (m)
h_D	fluid height in the degasser (m)
Δh_m	manometer reading (m)
h_r	height of riser (m)
h_t	vertical distance between manometer taps (m)
I_{av}	average irradiance inside the reactor (μE m^{-2} s^{-1})
I_k	constant in Eq. (1) (μE m^{-2} s^{-1})
I_{mean}	average irradiance (μE m^{-2} s^{-1})
$I_{normalized}$	normalized irradiance
I_o	irradiance on photobioreactor surface (μE m^{-2} s^{-1})
I_w	irradiance in the water pool (μE m^{-2} s^{-1})
k_La_L	volumetric gas–liquid mass transfer coefficient (s^{-1})
k_L	gas–liquid mass transfer coefficient (m s^{-1})
K_a	extinction coefficient for biomass (m^2 g^{-1})
K_B	frictional loss coefficient for the bottom zone of the airlift
K_T	frictional loss coefficient for the top of the airlift
L	straight tube length in loop (m)
L_D	length of the degasser section (m)
L_{eq}	equivalent length of solar loop (m)
L_t	distance between the tracer injection and detection points (m)
n	exponent in Eq. (1)
n_T	number of tube diameters of separation between adjacent tubes
$[O_2^*]$	saturation concentration of oxygen in liquid in equilibrium with gas phase (mol l^{-1})
$[O_2]_{in}$	dissolved oxygen concentration at entrance of solar tube (mol l^{-1})
$[O_2]_{out}$	dissolved oxygen concentration at the outlet of the solar tube (mol l^{-1})
P_{ba}	areal productivity of biomass (g m^{-2} d^{-1})
P_{bv}	volumetric productivity of biomass (g l^{-1})
Q_L	volumetric flow rate of liquid (m^3 s^1)
Q_R	volumetric rate of fluid interchange per unit tube length (m^2 s^{-1})
R_{O_2}	volumetric rate of oxygen generation (mol O_2 m^{-3} s^{-1})
s	length of arc in Fig. 4 (m)
t	time (s)
t_c	cycling time (s)
t_d	time spent in the dark zone (s)
t_f	time spent in the photic zone (s)
t_{mr}	time interval between tracer injection and detection (s)
U_b	terminal rise velocity of single bubble (m s^{-1})
U_G	gas velocity in the riser zone (m s^{-1})
U_L	superficial liquid velocity in the tube (m s^{-1})

U_{LL}	superficial liquid velocity at large-scale (m s^{-1})
U_{LD}	superficial liquid velocity in the degasser (m s^{-1})
U_{LS}	superficial liquid velocity at small-scale (m s^{-1})
U_R	radial velocity (m s^{-1})
U_{RL}	radial velocity at large-scale (m s^{-1})
U_{RS}	radial velocity at small-scale (m s^{-1})
V	total volume of reactor (m^3)
V_d	dark volume (m^3)
V_f	volume of light zone (m^3)
V_L	volume of liquid in a given zone (m^3)

Greek symbols

α	factor dependent on the illuminated volume fraction (Eq. (22))
β	ratio of superficial gas velocity to the total (gas and liquid) superficial velocity
ε_l	gas holdup in the loop
ε_r	gas holdup in the riser
ε_d	gas holdup in the downcomer
λ	characteristic parameter in Eq. (14)
μ	specific growth rate (h^{-1})
μ_L	viscosity of the culture broth (kg m^{-1} s^{-1})
μ_{max}	maximum specific growth rate (h^{-1})
v	light/dark cycle frequency (Hz)
ρ	density of the fluid (kg m^{-3})
σ	interfacial tension (J m^{-2})
ϕ	illuminated volume fraction of the solar collector (photic volume fraction)
ϕ_{eq}	length of light path in Eq. (4) defined by Eq. (5) (m)
ϕ_L	illuminated volume fraction of tube at large-scale
ϕ_S	illuminated volume fraction of tube at small-scale
θ	solar zenith angle in Eq. (5) (degrees)

1. Introduction

Culture of microalgae in open ponds and raceways is well developed but only a few species can be maintained in traditional open systems that control contamination by using highly alkaline or saline selective environments. Fully closed photobioreactors provide opportunities for monoseptic culture of a greater variety of algae than is possible in open systems. Of the many designs of closed photobioreactors that have been evaluated, devices with tubular solar collectors are the most promising (Molina Grima, 1999; Tredici, 1999). Tubular photobioreactors that circulate the culture by using an airlift device are especially attractive for several reasons: circulation is achieved without moving parts and this provides a robust culture system with a reduced potential for contamination (Chisti, 1989); the cell damage associated with mechanical pumping is avoided (Chisti, 1999a; Vandanjon et al., 1999); and the airlift device combines the function of a pump and a gas exchanger that removes the oxygen produced by photosynthesis (Camacho Rubio et al., 1999). Continuous removal of oxygen is essential, as excessive dissolved oxygen in the broth inhibits photosynthesis.

In an airlift driven tubular photobioreactor, the recirculation velocity of the culture and oxygen removal characteristics are closely linked. The culture performance is critically dependent on attaining an optimal design that provides the requisite flow and gas exchange. In addition, the photobioreactor geometry must maximize capture of sunlight while minimizing the land surface occupied (Acién Fernández et al., 1997). Here, we provide a method for designing airlift driven tubular photobioreactors with continuous run solar collectors. Effects of tube length, flow velocity, the airlift column height, and the geometric configuration of the solar receiver on various performance parameters are discussed. A photobioreactor designed using the approach outlined is proved for culture of the microalga *Phaeodactylum tricornutum*.

2. Photobioreactor design

An airlift driven tubular photobioreactor is shown in Fig. 1. The airlift column circulates the culture through the solar collector tubing where most of the photosynthesis occurs. The oxygen produced by photosynthesis accumulates in the broth until the fluid returns to the airlift zone where the accumulated oxygen is stripped by air. A gas–liquid separator in the upper part of the airlift column prevents gas bubbles from recirculating into the solar collector. The solar loop is designed to efficiently collect the solar radiation, minimize resistance to flow, and occupy minimal area to reduce the demand for land. In addition, the diameter of the solar tubing is selected so that the volume of the dark zone (i.e. one with light intensity below saturation) is kept to a minimum. Also, the interchange of fluid between the light and the dark zones in the solar loop must be sufficiently rapid that element of fluid do not reside continuously in the dark zone for long. How the various design requirements can be met is discussed next, initially by focusing on the solar collector and the airlift column separately.

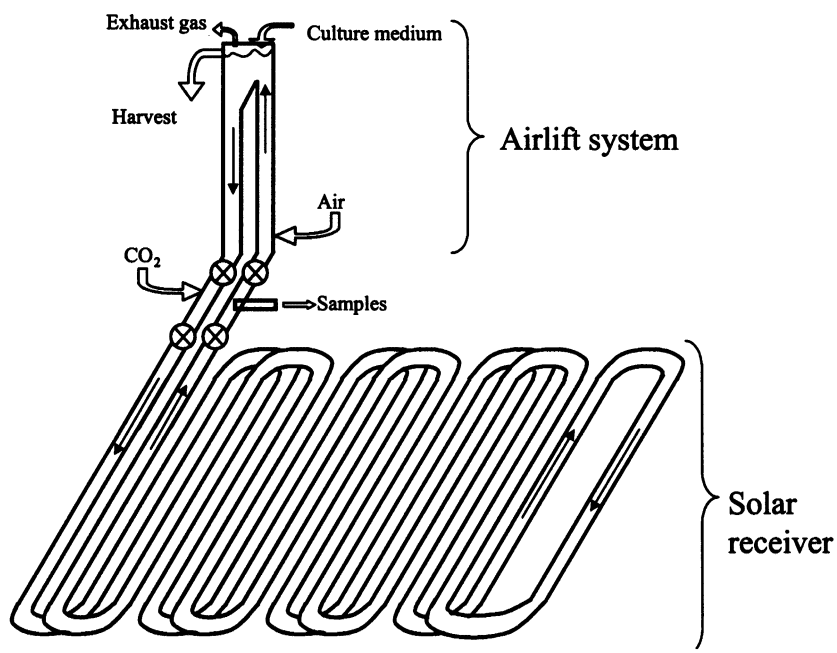

Fig. 1. The photobioreactor.

2.1. The solar collector

Biomass productivity is the variable that needs to be optimized in designing a photobioreactor for mass culture of microalgae. Production of biomass is controlled mainly by the availability of light. In continuous culture, the specific growth rate of biomass depends on the average irradiance in the solar tube. Various relationships have been developed for this dependence; a suitable relationship (Molina Grima et al., 1994a) for the alga of interest is:

$$\mu = \frac{\mu_{max} I_{av}^n}{I_k^n + I_{av}^n}, \quad (1)$$

where μ is the specific growth rate, μ_{max} is the maximum value of μ, I_{av} is the average irradiance inside the reactor, I_k is a constant dependent on algal species and culture conditions, and n is an empirically established exponent. Once the specific growth rate is known, the volumetric productivity of the biomass is easily calculated:

$$P_{bv} = \mu C_b, \quad (2)$$

where P_{bv} is the volumetric productivity and C_b is the concentration of the biomass in the harvest stream of the continuous flow bioreactor. The areal productivity P_{ba} is related with the volumetric productivity (Eq. (2)), as follows:

$$P_{ba} = P_{bv} \frac{\pi d_t^2}{4 n_T d_t} = P_{bv} \frac{\pi d_t}{4 n_T}, \quad (3)$$

where the separation between the adjacent parallel rungs of the continuous run looped tubing is expressed as a function of the tube diameter (i.e. separation $= n_T d_t$) with n_T being the number of tube diameters of separation between tubes. The selection of n_T value is based on empirical optimization, as discussed in Section 3.2. In an alternative method of calculating P_{ba}, the multiplier ($\pi d_t / 4 n_T$) in Eq. (3) is replaced with V/A, where V is the volume of the reactor and A is the land area occupied by it.

Estimation of μ and the productivity require a knowledge of the average irradiance I_{av}. This is evaluated using the well-known principles of astronomy (to establish the position of the Sun relative to the photobioreactor), solar power engineering (to determine the intensity of the incident radiation), and the Beer–Lambert relationship, as summarized elsewhere (Molina Grima et al., 1999). The average irradiance inside a culture (Alfano et al., 1986) is given by the equation:

$$I_{av} = \frac{I_o}{\phi_{eq} K_a C_b} [1 - \exp(-\phi_{eq} K_a C_b)], \quad (4)$$

where K_a is the extinction coefficient of the biomass, I_o is the irradiance on the culture surface, and ϕ_{eq} is the length of the light path from the surface to any point in the bioreactor. For outdoor placed tubular systems, ϕ_{eq} is related with the tube diameter (Acién Fernández et al., 1997); thus,

$$\phi_{eq} = \frac{d_t}{\cos\theta}, \quad (5)$$

where d_t is the tube diameter. Eq. (4) is independent of the nature of the radiation field around a reactor and is valid for all geometries. Thus, from a knowledge of the characteristics parameters of the algal strain (i.e. μ_{max}, K_a, I_k, and n) and using Eqs. (1)–(5), the biomass productivity may be determined for any combination of external irradiance and the diameter of solar collector tubes.

For otherwise fixed conditions, the geometric arrangement of the solar collector tubes also determines the irradiance on the surface of the tubes because the mutual shading by tubes is influenced by how they are arranged over a given surface area. A two-layered loop (Fig. 1), as used by Torzillo et al. (1993), maximizes efficiency of land use. The lower set of tubes is displaced horizontally relative to the upper one, so that all tubes are visible when viewed from directly overhead. In addition, the design must ensure that the flow in the solar tube is turbulent (i.e. the minimum Reynolds number should exceed 3000) so that the cells do not stagnate in the dark interior of the tube. At the same time, the dimensions of the fluid microeddies should always exceed those of the algal cells, so that turbulence associated damage is prevented. Methods for calculating the microeddy size in tubular flow are well known (Chisti, 1999a; Mirón et al., 1999). The need to control eddy size places an upper limit on the flow rate through the solar tubing.

Another restriction on the design of the solar collector is imposed by the rate of photosynthesis, the liquid velocity in the tube, and the acceptable upper limit on the concentration of dissolved oxygen (Camacho Rubio et al., 1999; Mirón et al., 1999). The maximum length L of a continuous run tube is constrained, as follows:

$$L = \frac{U_L([O_2]_{out} - [O_2]_{in})}{R_{O_2}}, \quad (6)$$

where U_L is the maximum permissible culture velocity established by the cell damage considerations. In Eq. (6), the oxygen concentration at the entrance of the solar tube is generally the same as the saturation value when the fluid is in equilibrium with the atmosphere. The concentration at the outlet, $[O_2]_{out}$, is the maximum acceptable value that does not inhibit photosynthesis. R_{O_2} is the volumetric rate of oxygen generation by photosynthesis in the tube.

2.2. The airlift circulator

The airlift device fulfills two needs: the circulation of the fluid through the solar loop and stripping of oxygen from the broth. The volume of the broth in the airlift device needs to be small compared to the volume in the solar loop so that the cells spend as much time as possible in the relatively better illuminated loop. In this work, the riser and downcomer tubes of the airlift device were vertical extensions of the ends of the solar loop. The volume in the gas–liquid separator was minimized by reducing the spacing between the parallel walls (Fig. 2) to the width of the riser (or the downcomer) tube (Fig. 1). The bottom of the separator was slanted at 60° relative to the horizontal, so that the solids would not settle permanently.

The head zone of the airlift column (Fig. 1) was designed for almost complete separation of the gas from the liquid, before the broth recirculated into the solar collector. Complete disengagement of gas meant that the driving force for liquid circulation was the maximum attainable for any aeration rate in the airlift riser. For disengagement of gas, the distance between the entrance and the exit of the separator zone

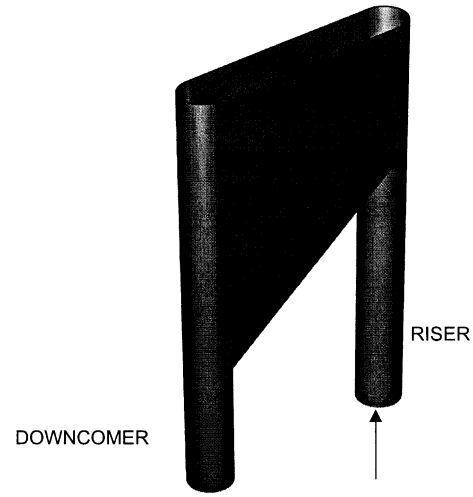

Fig. 2. The gas–liquid separator.

should be such that the smallest bubbles can rise out of the fluid by the time it exits the separator and moves into the downcomer (Chisti and Moo-Young, 1993). Thus, the time taken by the fluid to traverse the length of the degasser must be greater than or equal to time required by the bubbles to rise out. Because all fluid entering the degasser through the riser tube moves through the cross-section of the degasser, we have

$$U_L A_r = U_{LD} A_D, \quad (7)$$

where A_r is the cross-sectional area of the riser tube, A_D is the mean vertical cross-sectional area of the degassing zone, and U_{LD} is the mean superficial liquid velocity in the degasser. When the parallel degasser walls are spaced a distance d_t apart, the area A_D equals $h_D d_t$, where h_D is the mean height of fluid in the degasser zone. To satisfy the disengagement criterion (Chisti and Moo-Young, 1993), the length L_D of the degasser is governed by the relationship:

$$\frac{L_D}{U_{LD}} \geqslant \frac{h_D}{U_b}, \quad (8)$$

where U_b is the bubble rise velocity. Because $h_D = A_D/d_t$, substitution of Eq. (7) in Eq. (8) provides the following equation:

$$L_D = \frac{U_L A_r}{d_t U_b} = \frac{\pi d_t}{4}\frac{U_L}{U_b}. \quad (9)$$

A bubble rise velocity of 0.1 m s^{-1} was used in Eq. (9) to obtain the minimum length L_D.

The liquid flow in the solar receiver is driven by the airlift pump. For a waterlike fluid such as the microalgal broth, the induced flow velocity depends mainly on the geometric configuration of the circulation loop and the difference in gas holdup in the riser and the downcomer zones of the airlift column. This relationship has been established (Chisti, 1989) to be:

$$U_L = \sqrt{\frac{2g(\varepsilon_r - \varepsilon_d)h_r}{\frac{K_T}{(1-\varepsilon_r)^2} + K_B\left(\frac{A_r}{A_d}\right)^2\frac{1}{(1-\varepsilon_d)^2}}}, \quad (10)$$

where K_T and K_B are the frictional loss coefficients for the top and the bottom connecting sections, respectively, of the airlift loop. Eq. (10) is based on principles of energy conservation and it has been repeatedly validated for a broad range of scales and configurations of airlift devices (Chisti, 1989). In Eq. (10), h_r is the height of the riser zone, A_r and A_d are the cross-sectional areas of the riser and the downcomer, ε_r is the gas holdup in the riser, and ε_d is the holdup in the downcomer. In the present work, the entire solar collector constitutes the 'bottom zone'. In airlift devices generally, K_T is much smaller than K_B; hence K_T can be neglected (Chisti, 1989). This is particularly true of the loop configuration used for the photobioreactor (Fig. 1). Because the bottom of the airlift device is simply a continuous smooth pipe (the solar receiver) and the Reynolds number is always between 2.5×10^3 and 10^5, the frictional loss coefficient K_B can be approximated as

$$K_B = 0.3164\left(\frac{\rho U_L d_t}{\mu_L}\right)^{-0.25}\frac{L_{eq}}{d_t}, \quad (11)$$

where L_{eq} is the equivalent length of the loop, i.e. the straight tube length L plus additional length that provides the same pressure drop as all the bends and valves in the loop combined. Because no gas bubbles recirculate, $\varepsilon_d = 0$; hence Eq. (10) with the K_T term neglected and K_B replaced with Eq. (11) becomes:

$$U_L = \sqrt{\frac{g\varepsilon_r h_r}{0.3164\left(\frac{\rho U_L d_t}{\mu_L}\right)^{-0.25}\frac{L_{eq}}{d_t}}}. \quad (12)$$

For estimating U_L for any known riser gas holdup (ε_r), Eq. (12) is rearranged to:

$$U_L = \left(\frac{g\varepsilon_r h d_t^{1.25}}{0.3164\left(\frac{\mu_L}{\rho}\right)^{0.25}L_{eq}}\right)^{4/7}. \quad (13)$$

The gas holdup in the riser ε_r depends on the superficial velocities of the gas and liquid in the riser zone; these parameters are related according to the well-known Zuber and Findlay (1965) equation:

$$\varepsilon_r = \frac{\beta}{\lambda + \frac{U_b}{U_G + U_L}}, \quad (14)$$

where U_G and U_L are the superficial velocities of the gas and liquid in the riser zone, β is the ratio of the superficial gas velocity to the total superficial velocity, λ is a characteristic parameter, and U_b is the bubble rise velocity. The parameter λ is a function of the radial velocity profile; λ typically varies from 1.0 to 1.3 as the flow changes from turbulent to laminar. The bubble rise velocity U_b is a function bubble size. For the type of bubbles existing in the riser, the velocity tends to be between 0.2 and 0.4 m s^{-1}. Eqs. (13) and (14) are solved simultaneously to determine the holdup ε_r and the velocity U_L for any specified height h_r of the airlift column.

For estimating the oxygen removal capability of the airlift column, the overall gas–liquid volumetric mass transfer coefficient $k_L a_L$ may be estimated directly using various available correlations (Chisti, 1989, 1999b); however, the reliability of such estimates is often quite poor especially for unusual reactor geometries as was the case here. A more reliable prediction method based on fundamental principles and small-scale experimentation has been demonstrated for several cases (Chisti, 1989, 1999b) and that approach was used here. Thus, the volumetric mass transfer coefficient ($k_L a_L$), the gas holdup (ε_r), the mean bubble diameter (d_B), and the true mass transfer coefficient (k_L) are known to be related (Chisti, 1989) according to the equation:

$$\frac{k_L}{d_B} = \frac{k_L a_L (1-\varepsilon_r)}{6\varepsilon_r}. \quad (15)$$

Calculations of the k_L/d_B ratio (Eq. (15)) from the measured $k_L a_L$ and gas holdup in bubble columns and airlift devices have shown this ratio to be a constant for a given fluid, irrespective of the aeration rate (Chisti and Moo-Young, 1987; Chisti, 1989). For air–water dispersions and for suspensions in which the suspending fluid is waterlike, the value of k_L/d_B may be calculated (Chisti, 1989) with the equation:

$$\frac{k_L}{d_B} = 5.63 \times 10^{-5}\left(\frac{gD_L\rho^2\sigma}{\mu_L^3}\right)^{0.5} e^{-0.131C_S^2}, \quad (16)$$

where C_S is the concentration of solids in suspension (wt./vol.%), D_L is the diffusivity of gas in liquid, and σ is the interfacial tension. The k_L/d_B ratio calculated with Eq. (16) could be used in Eq. (15) to determine the $k_L a_L$. The gas holdup ε_r had been determined earlier using Eqs. (13) and (14).

2.3. Scale-up considerations

For practical purposes, the scale-up of a photobioreactor requires scaling up of both the solar receiver and the airlift device. Scale-up of the latter does not pose a limitation for any realistic size of the photobioreactor (Chisti, 1989); however, there are limitation to scaling up a continuous run solar loop. The solar loop is the productive part of the photobioreactor. In principle, the volume of the loop may be increased by increasing the diameter and the length of the tube. In practice, only the tube diameter may be varied because the maximum length is constrained (Eq. (6)), as discussed earlier. Any change in tube diameter would imply a change in the relative volumes of the dark and the light zones. Under given conditions (i.e. the solar irradiance, the biomass concentration and pigment content), the depth at which the light intensity declines to a growth limiting value would not be affected by an increase in tube diameter, but the depth of the dark zone would increase. Productivity of the reactor will deteriorate on scale-up unless the frequency of the light/dark interchange is held constant. If the light/dark cycling time is allowed to increase, the productivity will begin to decline as soon as the cycling time exceeds a maximum value. Evidence suggests that the minimum acceptable value of the light/dark cycle frequency of *P. tricornutum* culture is about 1 s^{-1} (Molina Grima et al., 2001); lower values of frequency reduce culture productivity, as shown in Fig. 3 for various mean irradiance values. Therefore, the diameter of the solar tube should be such that at the maximum permissible (or practicable) velocity in the tube the cycle frequency does not reduce to below 1 s^{-1}.

To quantify the light/dark cycling time inside the culture, the light distribution and the velocity at which the cells are moving within the reactor need to be determined. The photic volume (i.e. the volume that is not photolimited) of the culture may be established by calculating the light profiles in the tube (Acién Fernández et al., 1997), as in Fig. 4. The dark volume (i.e. the total volume minus the photic volume) is similarly determined and this allows the calculation of the fraction of the tube volume that is illuminated to above the saturation light intensity. The entire dark volume of the culture must move to the photic zone within a short time. A volumetric rate of fluid movement out of the dark zone (Q_R) may be defined as follows:

$$Q_R = \frac{\text{dark zone volume}}{t_d}, \quad (17)$$

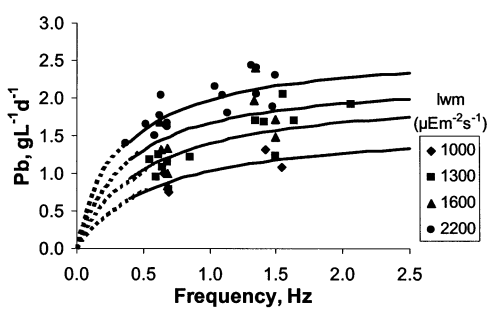

Fig. 3. Variation of volumetric biomass productivity with the light–dark cycling frequency and the external mean irradiance. The data shown spanned the following conditions: $0.241 \leqslant U_L$ (m s^{-1}) $\leqslant 0.500$; $0.025 \leqslant D$ (h^{-1}) $\leqslant 0.500$; d_t (internal) values of 0.025 and 0.053 m; 20 ± 2 °C culture temperature; and a pH of 7.7.

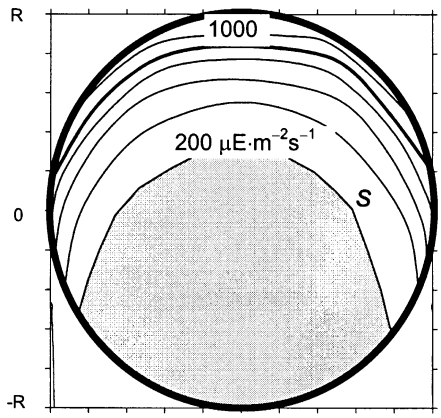

Fig. 4. Irradiance profiles inside the solar collector tube at midday and for a dilution rate of 0.04 h^{-1}. The tube diameter was 0.06 m.

where t_d is the maximum acceptable duration of the dark period between successive light periods. The Q_R value in Eq. (17) is on a unit tube length basis. Because all the fluid moving out of the dark zone must pass through the boundary between the light and the dark zones (Molina Grima et al., 1999), a fluid interchange velocity (U_R) can be defined as follows:

$$U_R = \frac{Q_R}{s}, \tag{18}$$

where s is the length of the boundary arc between the two zones (Fig. 4).

To ensure identical performance at the two scales, the light/dark cycling time t_c, i.e. the sum of the time spent by the cells in the photic and the dark zones at the two scales should be held constant. That is, $t_c = t_f + t_d$ should be constant, where t_f and t_d are the times in the photic and the dark zones, respectively. The light (t_f) and dark periods (t_d) are determined by the cycle frequency, v, which is equal to $1/(t_f + t_d)$. As previously noted, for a known level of external irradiance, biomass concentration, and absorption coefficient of the biomass, the fractional culture volume ϕ that is illuminated (i.e. the photic volume fraction) can be estimated from the light profiles; $\phi = V_f/(V_f + V_d)$. If we assume that the volume V_f is proportional to the flash period t_f, and the dark volume V_d is proportional to the dark period t_d, the cycling time t_c can be expressed in terms of ϕ, as follows:

$$t_c = t_d\left(\frac{1}{1-\phi}\right). \tag{19}$$

Thus, the frequency v is:

$$v = \frac{1-\phi}{t_d}. \tag{20}$$

To ensure identical performance at the two scales, the light/dark cycling frequency at the two scales should be the same. Using these equations, the light/dark interchange velocity at large-scale (U_{RL}) and that at the small-scale (U_{RS}) may be shown (Molina Grima et al., 2001) to depend on the scale factor f, as follows:

$$U_{RL} = \frac{f}{\alpha}U_{RS}. \tag{21}$$

The factor f is simply the ratio of the tube diameters at the larger and the smaller scales. The parameter α in Eq. (21) depends on the ϕ values at the two scales; thus,

$$\alpha = \left(\frac{1-\phi_L}{1-\phi_S}\right). \tag{22}$$

The interchange velocity U_R is estimated as the fluctuating component of the steady-state velocity (Molina Grima et al., 2001) in turbulent flow:

$$U_R = 0.2\left(\frac{U_L^7\mu}{d_t\rho}\right)^{1/8} \tag{23}$$

which allows the calculation of the radial velocity (U_R) in the turbulent core as a function of the superficial liquid velocity (U_L), the tube diameter (d_t), and the density (ρ) and viscosity (μ) of the culture broth. Successful scale-up demands that the linear flow velocities at the two scales conform to the following equation (Molina Grima et al., 2001):

$$U_{LL} = \frac{f^{9/7}}{\alpha^{8/7}}U_{LS}. \tag{24}$$

3. Materials and methods

3.1. Organism and nutrient medium

P. tricornutum UTEX 640 was the microalga used. The culture was obtained from the collection of the University of Texas, Austin. *P. tricornutum* is a freshwater alga that tolerates a high salinity (Yongmanitchai and Ward, 1991). The inoculum for the photobioreactors was grown indoors under artificial light (230 μE m^{-2} s^{-1} light flux at the vessel's surface) in a 20 l bubble column. Mann and Myers (1968) medium was used to produce the inoculum. The culture temperature was 20 °C.

3.2. Outdoor photobioreactor

The optimally designed tubular photobioreactor (Fig. 1) consisted of a 4 m tall airlift section with a degasser zone (Fig. 2). Air was injected in one of the vertical tubes, or the riser, of the airlift device. The two ends of a continuous run solar receiver tubing were connected to the airlift riser and downcomer pipes, respectively. The internal diameter of the tubing of the solar loop, the riser, and the downcomer was the same at 0.053 m. The external tube diameter was 0.06 m. The total reactor volume was 0.2 m^3. The airlift zone comprised ~ 0.023 m^3, or less than 12% of the total volume, so that the time spent by the culture in the solar collector could be maximized.

The continuous run solar collector tubing was arranged in two layers (Fig. 1) and the total run length was 80 m. The solar loop occupied an area of 12 m^2. The adjacent intertube distance in any horizontal plane was 0.09 m (Fig. 5). The wall-to-wall vertical distance between the two layers of the loop was 0.03 m. The length of the degasser zone was 0.22 m and its bottom was sloped at an angle of 60° to the horizontal (Fig. 2). The photobioreactor was made of Plexiglas. The solar receiver loop was submerged in a pond of water held at 20 ± 2 °C. The reactor was located in Almería (36°50′N, 2°27′W), Spain.

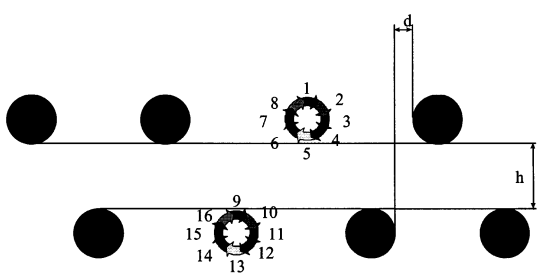

Fig. 5. Solar loop geometry. The vertical distance *h* and the horizontal spacing *d* between tubes are shown. Eight measurement points are indicated on the perimeter of tubes for averaging the irradiance received values.

The optimal placement of solar receiver tubes was established empirically by arranging 0.06 m diameter tubes with blackened surfaces in the configuration of the solar loop and measuring the irradiance on the tube perimeter at eight equally spaced locations on tubes in both planes (Fig. 5). The measurements were averaged to obtain a mean value, I_{mean}. Irradiance I_w was measured also on the surface of the water pool. The mean irradiance on the surface of a tube was normalized with respect to that on the water pool, to obtain a dimensionless irradiance $I_{normalized}$. Measurements were made for a total of 18 combinations of vertical distance *h* and the horizontal tube spacing *d* (Fig. 5). The *d*-values tested were 0, 0.03, 0.06, 0.09, 0.12, and 0.15 m; the *h*-values were 0, 0.03, and 0.06 m.

3.3. Solar irradiance measurement

The photosynthetic photon flux fluence rate or quantum scalar irradiance I_w, was measured periodically inside the pond using a quantum scalar irradiance meter (QSL-100 Biospherical Instruments Inc., San Diego, CA). This type of sensor measures the photon flux from all directions and it is better suited for systems that operate independently of the geometry of the light field. Because phytoplankton are scalar collectors, and photosynthesis does not depend on the direction from which the photons are received, scalar irradiance is a better measure of the available photon flux.

The light profiles within the culture were estimated using a published model of irradiance (Acién Fernández et al., 1997), measured biomass concentration, and the culture absorption coeffi-

cient K_a. The irradiance profiles inside tubes could be used to demarcate the cross-section of the solar receiver tubes into a 'dark' zone with irradiance values below saturation, or ~ 185 μE m^{-2} s^{-1} (Mann and Myers, 1968; Acién Fernández et al., 1998); the rest of the cross-section was the photic zone.

3.4. The liquid velocity and gas holdup

The liquid velocity in the tube was measured by the tracer method. Thus, a pulse of acid/alkali was introduced at the entrance of the tubular loop and detected at the end using a pH electrode. The liquid velocity, U_L, was calculated using the known distance L_t between the tracer injection and detection points (entrance and exit of the solar collector), and the measured time interval between injection and detection. Thus,

$$U_L = \frac{L_t}{t_{mr}}, \tag{25}$$

where the time interval t_{mr} was obtained as follows

$$t_{mr} = \frac{\int_0^\infty tC\,dt}{\int_0^\infty C\,dt}. \tag{26}$$

In Eq. (26), C was the concentration of the acid tracer, measured with a pH electrode.

The gas holdup in the riser was measured by the manometric method (Chisti, 1989). Thus, two pressures taps drilled near the top and the bottom of the riser section were connected to an inverted U-tube manometer. From the known vertical distance h_t between the taps, and the manometer reading Δh_m, the holdup was calculated as follows:

$$\varepsilon_r = \frac{\Delta h_m}{h_t}. \tag{27}$$

Because visible gas bubbles did not recirculate, the gas holdup in the downcomer and the loop were negligible, except when gas was injected in the loop. In the latter case, the gas holdup in the loop was estimated as the ratio of the gas flow rate and the total (gas and liquid) fluid flow in the tube.

3.5. Volumetric mass transfer coefficients

The volumetric gas–liquid mass transfer coefficient was determined in seawater without the cells. The reactor was filled with seawater and liquid circulation was initiated by supplying air in the riser, as in normal culture operations. Once a steady state had been attained, the water became air saturated and the measured concentration of dissolved oxygen was constant at the entrance (i.e. in the degasser zone) and the exit of solar collector. At this point, nitrogen was injected at the inlet of the solar tube. The location of the nitrogen injection point and the flow rate of the gas were identical to those used typically during culture for supplying carbon dioxide for pH control. Because of stripping of dissolved oxygen by the nitrogen gas, the oxygen concentration at the exit of the solar tube declined continuously until a new steady state had been attained (Camacho Rubio et al., 1999). At this condition, the amount of dissolved oxygen stripped in the solar receiver equaled the amount of oxygen absorbed in the airlift pump (riser and degasser). An oxygen mass balance on the solar receiver could now be established (Camacho Rubio et al., 1999) as follows:

$$Q_L([O_2]_{in} - [O_2]_{out}) = V_L k_L a_L([O_2^*] - [O_2])_{LM}(1 - \varepsilon_l). \tag{28}$$

In view of the plug flow regime, Eq. (28) employs a logarithmic mean driving force for oxygen transfer, calculated in the usual way (Camacho Rubio et al., 1999). The dissolved oxygen values at the inlet and the outlet of the solar tube were determined experimentally, whereas the equilibrium dissolved oxygen values were estimated using Henry's law. Similar balances could be established for the airlift pump and, hence, the $k_L a_{L,airlift}$ in the airlift device (excluding the solar collector) could be determined (Camacho Rubio et al., 1999).

3.6. Operating mode

The outdoor photobioreactor was operated as a chemostat; the steady-state dilution rates ranged from 0.037 to 0.061 h^{-1}. The liquid velocity in the solar tube varied independently of the dilution

Table 1
Biomass concentrations and productivities for various dilution rates, liquid velocities, and solar irradiance levels during cultures in the designed reactor

Date	D (h^{-1})	U_L (m s^{-1})	I_w (μE m^{-2} s^{-1})	C_b (g l^{-1})	P_{bv} (g l^{-1} d^{-1})	P_{ba} (g m^{-2} d^{-1})
24/7	0.037	0.40	2690	4.10	1.52	25.3
31/7	0.048	0.40	2596	3.96	1.90	31.7
5/8	0.061	0.40	2548	2.70	1.65	27.4
30/3	0.050	0.50	1289	2.38	1.19	19.8
5/4	0.050	0.35	1126	2.29	1.15	19.1
8/4	0.050	0.17	1250	–	–	–

rate, from 0.17 to 0.50 m s^{-1}. The liquid velocity was varied by changing the superficial aeration velocity in the riser tube, over the range of 0.005–0.031 m s^{-1}. At any given dilution rate, fresh medium was added during a 10-h daylight period and dilution stopped during the night until biomass concentration at sunrise remained unchanged for four consecutive days. The cultures were maintained at pH 7.7 by automatically injecting carbon dioxide, as needed, in response to a pH controller. The carbon dioxide flow rate was sufficiently low that only microbubbles were produced. Nutrient limitations were prevented by using the Mann and Myers (1968) medium at three times the normal concentration.

3.7. Photosynthetic activity

The photosynthetic activity of the cells was measured using a method similar to that described in the past (Vonshak et al., 1985). Thus, the oxygen generation rate was determined under controlled indoor conditions of samples from the outdoor reactor. Culture samples were diluted to an optical density (OD) of 0.1 at 625 nm, brought to 22 °C in a 1 l thermostated vessel, and irradiated at 2000 μE m^{-2} s^{-1} by a halogen lamp located 0.5 m from the front of the vessel. Dissolved oxygen was measured (Lisle-Metrix 2200D/P91, dissolved oxygen electrode) every second over a 30 min period and recorded automatically. During the measurements, the culture was mixed using a magnetic stirrer. The photosynthetic activity of the cells was determined as the rate of change in dissolved oxygen concentration.

3.8. Biomass concentration

The biomass concentration was estimated hourly during daylight from the measured OD of the culture. The OD was measured spectrophotometrically (Hitachi U-1000 spectrophotometer) at 625 nm wavelength in a cuvette with 1 cm light path. The spectrophotometric determinations of biomass were periodically verified by dry weight measurements on samples that had been centrifuged ($1800 \times g$), washed with 0.5 M hydrochloric acid and distilled water to remove non-biological adhering materials such as mineral precipitates, and freeze dried.

4. Results and discussion

4.1. Design of the reactor

Eqs. (1)–(5) were used to predict the mean annual biomass productivity of *P. tricornutum* at the known optimal dilution rate of 0.048 h^{-1}, using previously established (Acién Fernández et al., 1998) outdoor growth parameters for various conditions of irradiance and solar tube diameters. As the tube diameter increased, the volumetric productivity of the biomass declined for otherwise fixed conditions; however, the areal productivity increased as more culture volume could be accommodated in a given area. Thus, to attain a compromise between the conflicting demands of volumetric and areal productivities, a solar tube diameter value of 0.06 m was selected for construction. The estimated annual mean areal pro-

ductivity for the selected tube diameter was 35 g m^{-2} d^{-1}; the estimated volumetric productivity of biomass was 1.5 g l^{-1} d^{-1}. These values compared well with the measured data shown in Table 1.

Regarding the spacing of the adjacent tubes in the solar collector (Fig. 5), the normalized irradiance was not very sensitive to the vertical distance h, but the irradiance increased as the d-value increased from 0 to about 0.1 m. Once a d-value of 0.1 m had been attained, further increases did not significantly affect the radiation received. The optimal d and h values were 0.09 and 0.03 m, respectively, and these were used in constructing the solar collector. The selected configuration reduced surface irradiance on tubes by only 17% compared to the single layer, parallel run configuration with widely spaced tubes, as previously used by Molina Grima et al. (1994b). However, the multilayer design substantially enhanced the areal productivity relative to the single layer collector.

As previously noted, excessive turbulence is potentially damaging to a variety of algae (Chisti, 1999a). For *P. tricornutum*, a decline in specific-growth rate has been reported when the estimated dimensions of the microeddies are 45 μm and smaller (Contreras Gómez et al., 1998). If a lower safe limit on eddy length of 50 μm is accepted, the maximum culture velocity cannot exceed 1.0 m s^{-1}, as shown in the past (Acién Fernández et al., 2001). Although the estimated upper limit on acceptable velocity was 1.0 m s^{-1}, the design value was lower at 0.5 m s^{-1} because of limited mechanical strength of the plastic tubes. For this value of the velocity, the Reynolds number in the tube was about 26 000; the maximum tube length was calculated for an outlet concentration of dissolved oxygen of 300% of air saturation. The latter value had been shown to be acceptable in earlier work (Acién Fernández et al., 1998; Camacho Rubio et al., 1999). Thus, a maximum oxygen generation rate of 0.003 mol O_2 m^{-3} s^{-1}, corresponding to a biomass productivity of 2.5 g l^{-1} d^{-1} (Acién Fernández et al., 1998) was used in Eq. (6) to obtain a maximum solar collector length of 80 m (Fig. 6), for an assumed oxygen concentration of 100% of air saturation at the entrance of the collector tube.

The height of the airlift column required for attaining a flow velocity of 0.5 m s^{-1} was estimated using Eqs. (13) and (14). For any reasonable gas flow rate in the riser, the requisite liquid velocity could not be attained with an airlift column that was less than 4 m tall. Thus, a 4-m airlift height was selected for construction. Also, for a 4-m tall airlift, the estimates based on Eqs. (13)–(16) showed that a $k_L a_L$ value of 0.13 s^{-1} was easily attainable. This value of $k_L a_L$ in the airlift column was estimated as being sufficient for reducing the dissolved oxygen concentration from 300% of air saturation to less than 150% of air saturation at the entrance of the solar collector.

4.2. Hydrodynamic and mass transfer characterization

Once the photobioreactor had been built, its hydrodynamic and mass transfer behavior was characterized to validate the design approach used. Thus, the experimental measurements of the induced liquid velocity, gas holdup in the riser, and the $k_L a_L$ values are compared with predictions in Fig. 7 for various values of the superficial aeration velocity in the riser. The predictions agree exceptionally well with the measurements, confirming the reliability of Eqs. (13)–(16).

4.3. Outdoor culture

The microalga *P. tricornutum* was cultured outdoors under different conditions of solar irradi-

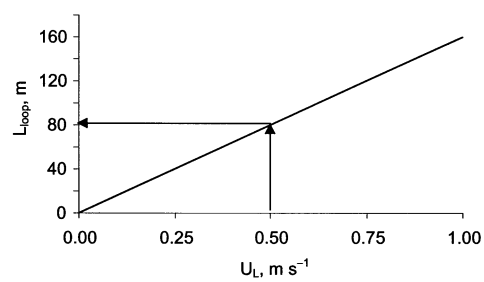

Fig. 6. Effect of liquid velocity on the maximum allowable length (Eq. (6)) of solar tube, if dissolved oxygen concentration in the fluid leaving the tube is not to exceed 300% of air saturation. Length was calculated with Eq. (6) for a volumetric photosynthesis rate value of 0.003 mol O_2 m^{-3} s^{-1}.

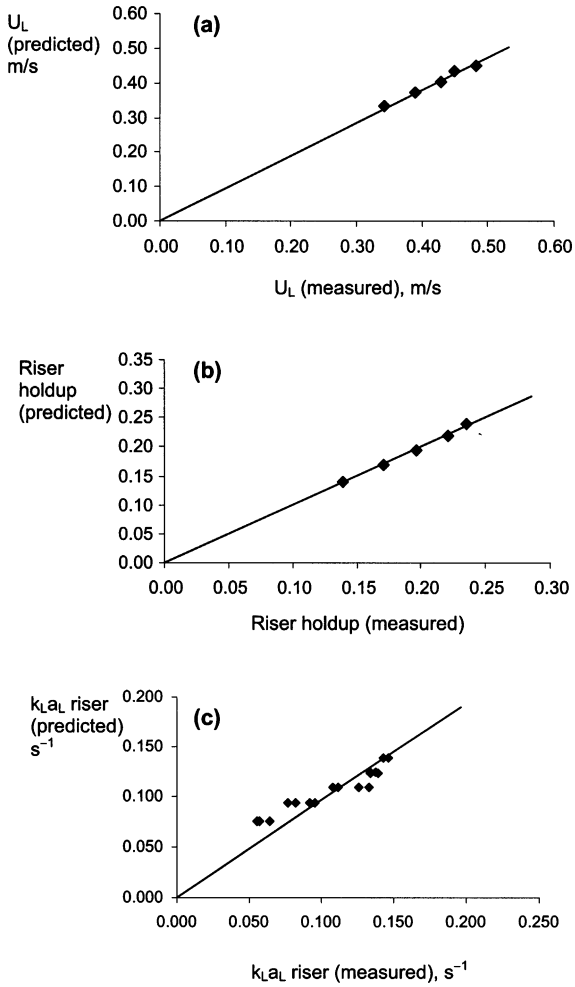

Fig. 7. Comparison between the model predicted and the experimental values of: (a) the riser liquid velocity; (b) the gas holdup in the riser; and (c) the k_La_L in the airlift riser.

ance, dilution rates, and liquid velocities in the loop. Some representative data are noted in Table 1. A maximum biomass productivity of 1.90 g l^{-1} d^{-1} was obtained at a dilution rate of 0.048 h^{-1} in the summer when the mean external irradiance (I_w) value was about 2600 μE m^{-2} s^{-1}. In the spring, the mean irradiance was lower, about 1200 μE m^{-2} s^{-1}, hence the biomass productivity declined to 1.20 g l^{-1} d^{-1}. The experimentally obtained biomass productivity of 1.9 g l^{-1} d^{-1} was about 10% greater than the value estimated using the design methodology. A similar level of agreement was seen between the predicted and measured areal productivities of biomass, thus, validating the predictive capability of the design equations.

To assess the influence of the solar loop liquid velocity on the culture performance, three different liquid velocities were tested: 0.50, 0.35, and 0.17 m s^{-1}. In all cases, the dilution rate was constant at an optimal value of 0.050 h^{-1}. At the highest liquid velocity, the biomass concentration attained was 2.38 g l^{-1}. A lower concentration of 2.29 g l^{-1} was obtained when the velocity was reduced to 0.35 m s^{-1}; however, the biomass productivity at these two velocities did not differ significantly. The culture carried out at a velocity of 0.17 m s^{-1} failed to attain steady state; the culture perished when the velocity was reduced further. Turbulence is known to enhance biomass productivity relative to laminar flow conditions. For example, Carlozzi and Torzillo (1996) noted a lower biomass productivity in laminar flow relative to that in turbulent conditions for *Spirulina* cultures in tubular photobioreactors. A 29% increase in *Spirulina* biomass productivity was observed when the flow pattern changed from laminar to turbulent in straight tubes. Further improvement in turbulent mixing produced no beneficial effect; a high liquid velocity of 0.97 m s^{-1} damaged the culture and reduced the biomass productivity. Similar beneficial effects of limited turbulence have been also observed for *Spirulina* in open ponds (Richmond and Vonshak, 1978). In other similar work, the yield of *Chlorella* growing in a tubular photobioreactor was enhanced when the flow pattern shifted from laminar to turbulent (Pirt et al., 1983).

Turbulence repeatedly moves cells from darker interior of a tube to the better illuminated peripheral zone, hence the cells are not starved of light for extended periods. Also, movement of cells from light to dark zones may actually enhance productivity so long as the duration of a dark period remains small. Dark intervals of the order of 1 s are said to improve of the solar energy conversion by biomass (Terry, 1986; Laws et al., 1987), as such intervals allow the dark catalytic reactions of photosynthesis to run to completion, restoring the photosynthetic apparatus to its full

efficiency for the next light period. With *P. tricornutum* too, the biomass productivity increased with enhanced turbulence. Thus, as shown in Table 1, the biomass productivity during spring was a little better at a higher flow velocity of 0.50 m s^{-1} compared to when the velocity was 0.35 m s^{-1}. As previously noted, the culture collapsed when the velocity was reduced to below 0.17 m s^{-1}, apparently because of photooxidation effects.

Despite the high biomass concentrations attained under suitable conditions and the fairly turbulent conditions used, the cultures experienced photoinhibition, especially at midday as shown in Fig. 8 where the photosynthetic activity of the cells, expressed as oxygen production rate, is plotted against the solar hour. Between 08:00 and 12:00 h, the photosynthetic activity increases because of increasing irradiance (Fig. 8); however, the activity declines between 12:00 and 14:00 h, when the sunlight is intense and the culture is photoinhibited. During 14:00 and 16:00 h, the photosynthetic activity recovers as the irradiance declines. The existence of photoinhibition under intense illumination is of course well documented for algal cultures and has been taken into account in the earliest growth models such as those of Aiba (1982). Easily implemented and inexpensive methods are needed for preventing loss of culture performance during periods of intense sunlight in outdoor culture. These methods should not reduce culture productivity and should be capable of being automated for large-scale production facilities.

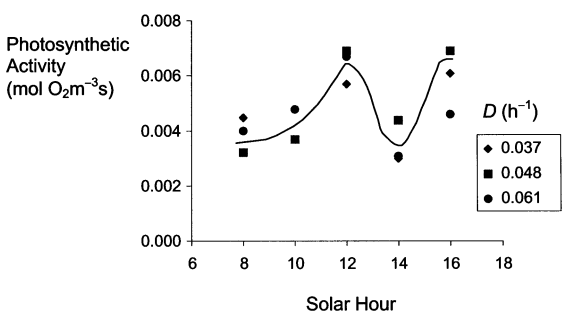

Fig. 8. Variation of the photosynthetic activity (i.e. the volumetric oxygen generation rate) of cells with the solar hour. Data were obtained during summer at three different dilution rates, *D*.

In addition to photoinhibition, another problem in continuous run tubular photobioreactors is the accumulation of dissolved oxygen that may reach inhibitory concentrations. High oxygen concentrations combined with intense sunlight may damage the cells by photooxidation. Potentially, the gas exchange requirements for removing the oxygen are a bigger constraint than for supplying carbon dioxide (Weissman et al., 1988). Photooxidation can severely affect the culture yield. Thus, Tredici et al. (1992) showed that the productivity of outdoor cultures of *Spirulina* was enhanced by reducing the dissolved oxygen concentration to 20 mg l^{-1} compared to when the concentration was 35 mg l^{-1}. It was further shown that for high productivity a low dissolved oxygen concentration must be combined with sufficiently intense turbulence (light availability). In studies with *Isochrysis galbana* grown outdoors in a glass column at different biomass concentrations, Qiang and Richmond (1994) observed that when cultures with relatively low population densities were exposed to full sunlight, the oxygen generation rate was low, implying photoinhibition or other stress on cells. Cultures with population densities significantly below optimal were lost within a few hours because of photooxidative death (Abeliovich and Shilo, 1972). Once the cells died, the chlorophyll was lost completely in another few hours.

The dissolved oxygen concentration in culture varies with solar hour, as shown in Fig. 9 for various dilution rates and culture velocities in the solar tube for summer and spring seasons. The variations in dissolved oxygen concentration are a reflection of the changes in the photosynthetic activity (oxygen generation) due to changes in the irradiance level. Thus, during 04:00 and 09:00 h, the dissolved oxygen concentration increases rapidly by up to 200% of air saturation as irradiance increases to around 1500 μE m^{-2} s^{-1}. At midday, when the irradiance level exceeds 1500 μE m^{-2} s^{-1}, the dissolved oxygen declines because of a reduced rate of generation (photoinhibition). In the afternoon, as the solar irradiance decreases, the dissolved oxygen concentration also reduces (Fig. 9).

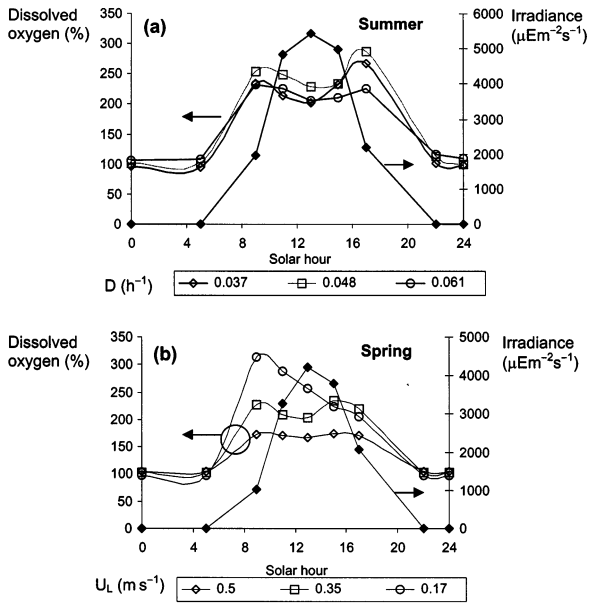

Fig. 9. Variation of solar irradiance and the dissolved oxygen concentration in the degasser zone with the solar hour. Data are shown for: (a) three different dilution rates in the summer; and (b) three different liquid velocities during spring.

As shown in Fig. 9, the culture behaves somewhat differently in spring than it does during the summer. The midday decline in dissolved oxygen concentration is lower during spring compared to in summer. This is because photoinhibition is less in the spring when the irradiance is generally lower than in summer. In addition, for the culture carried out at the highest liquid velocity of 0.50 m s^{-1}, the dissolved oxygen profile during the midday hours is flat without a distinct decline (Fig. 9(b)) whereas at a lower flow velocity of 0.35 m s^{-1} a clear midday dip is seen in the dissolved oxygen profile. As expected, oxygen accumulation is reduced at higher culture velocities in the solar tube. At the lowest flow velocity of 0.17 m s^{-1}, the dissolved oxygen concentration peaks at 300% of air saturation and, subsequently, declines (Fig. 9(b)). This suggests that the culture has been damaged, apparently by photooxidation occurring when a high concentration of oxygen combines with intense irradiance. At the lower flow rate, the cells experience the combined high oxygen and high irradiance environment for longer periods because of the longer time needed to traverse the solar loop. (A dissolved oxygen concentration of 300% of air saturation (i.e. 63% oxygen in gas in Fig. 10) negatively impacts cells even under conditions of low irradiance, as demonstrated by direct evidence in Fig. 10.)

The effect of dissolved oxygen on culture performance was further studied indoors (Fig. 10) under conditions of stable but reduced irradiance (300 μE m^{-2} s^{-1}) that eliminated any possibility of photooxidation. The culture in Fig. 10 was bubbled with a gas mixture containing nitrogen and oxygen in various proportions. The steady-state biomass concentration and oxygen generation rates obtained for different amounts of oxygen in the aeration mixture are shown (Fig. 10). Clearly, the dissolved oxygen concentration by itself influences the photosynthetic activity (oxygen generation rate) and the steady-state concentration of the biomass. The cultures in Fig. 10 were carried out at a dilution rate of 0.025 h^{-1}. Photosynthetic activity was reduced once the dissolved oxygen concentration exceeded 100% of air saturation, i.e. 21% oxygen in the aeration gas

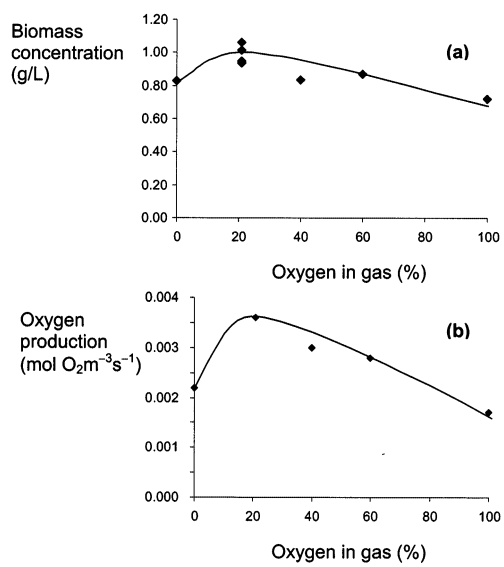

Fig. 10. Influence of the oxygen molar fraction in the injected gas on: (a) the steady-state biomass concentration; and (b) the photosynthetic activity (i.e. the volumetric oxygen generation rate) in indoor cultures. The dilution rate and the irradiance level were 0.025 h^{-1} and 300 μE m^{-2} s^{-1}, respectively.

(Fig. 10). The 100% oxygen in the aeration gas in Fig. 10 corresponds to a dissolved oxygen concentration of about 470% of air saturation. Whereas high oxygen concentrations inhibit photosynthesis, they do not cause cell death under conditions of low indoor irradiance.

As shown in Fig. 9(b), at the lowest liquid velocity (0.17 m s^{-1}) the culture reached a peak dissolved oxygen concentration of 300% of air saturation and thereafter, the oxygen concentration declined continuously as the cells died. In contrast, under indoor conditions a stable steady-state cell population was maintained even when bubbling with pure oxygen (Fig. 10). Obviously, a combination of oxygen inhibition and photooxidation is more damaging than inhibition by oxygen alone.

A simulation of the dissolved oxygen concentration at the end of the solar loop showed that as the oxygen generation rate (photosynthetic productivity) increased the dissolved oxygen concentration at the outlet increases (Camacho Rubio et al., 1999). Similarly, for a fixed photosynthetic productivity, the outlet dissolved oxygen concentration increased as the culture velocity was reduced. This is consistent with observations in Fig. 9. During summer with the most productive cultures, the dissolved oxygen concentration at the end of the solar loop may reach close to 400% of air saturation at a circulation velocity of 0.5 m s^{-1}.

4.4. Scale-up of the solar collector

As explained in a previous section, the light/dark cycling frequency in a solar collector affects the biomass productivity (Fig. 3). In principle, a solar collector tube with an increased diameter should be as productive as a narrower bore collector so long as the two devices have an identical value of the light/dark cycle frequency. For *P. tricornutum* the cycle frequency must be greater than 1 Hz in an optimally productive solar collector. If the volume of culture in the solar collector is doubled by increasing the diameter of the tube, the larger tube would require a diameter that is a factor of $\sqrt{2}$ greater than the diameter of the smaller tube. Even for this limited twofold increase in volume, it may be impossible to attain a light/dark cycle frequency of ~ 1 Hz, or greater, because of a shear-sensitivity imposed limit on the maximum acceptable velocity through the tube. Under these conditions, practicable scale-up may be possible only by enhancing the radial movement of fluid in the larger tube, for example, by modifying the design to include static flow promoters. Preferably, the flow promoters should be transparent and they should be spaced as far apart in the tube as possible. In practice, a doubling of the culture volume may be achieved by increasing the diameter by a factor of less than $\sqrt{2}$. This is because the larger tube would have a greater linear velocity and for it to have the same fluid residence time as the smaller tube (i.e. identical conversion or production in two tubes), the length would need to be greater.

5. Concluding remarks

A systematic method is discussed for engineered design of airlift driven photobioreactors with continuous run tubular solar collectors. The design method effectively combines the relevant aspects of external irradiance-dependent cell growth, oxygen accumulation in the solar loop, oxygen removal in the airlift device, and hydrodynamics of the airlift system that determine the flow velocity through the solar receiver. A 0.2 m^3 photobioreactor designed using the proposed method was evaluated in continuous outdoor culture of the microalga *P. tricornutum*. The model predicted hydrodynamic behavior of the bioreactor and the culture productivity agreed closely with the measured performance. The optimal bioreactor configuration and operations conditions were: a solar receiver tube of 0.06 m diameter, 80 m long, connected to a 4 m tall airlift; the solar tube was looped into two layers stacked 0.03 m apart; the optimal horizontal spacing between adjacent parallel rungs in any layer was 0.09 m. The solar collector occupied an area of 0.12 m^2. The culture velocity through the solar collector was about 0.5 m s^{-1}, but this could have been significantly higher. The parameter values used in modeling the bioreactor's performance are summarized in Table 2.

Table 2
The model parameter values used in bioreactor performance validation

Parameter	Value
λ	1.1
U_b (m s^{-1})	0.4
n	1.49
n_T	1.5
μ_{max} (h^{-1})	0.063
I_k (μE m^{-2} s^{-1})	114.67
K_a (m^2 g^{-1})	0.0369

References

Abeliovich, A., Shilo, M., 1972. Photooxidative death in blue–green algae. J. Bacteriol. 111, 682–689.

Acién Fernández, F.G., García Camacho, F., Sánchez Pérez, J.A., Fernández Sevilla, J.M., Molina Grima, E., 1997. A model for light distribution and average solar irradiance inside outdoor tubular photobioreactors for the microalgal mass culture. Biotechnol. Bioeng. 55, 701–714.

Acién Fernández, F.G., García Camacho, F., Sánchez Pérez, J.A., Fernández Sevilla, J.M., Molina Grima, E., 1998. Modelling of biomass productivity in tubular photobioreactors for microalgal cultures: effects of dilution rate, tube diameter and solar irradiance. Biotechnol. Bioeng. 58, 605–616.

Acién Fernández, F.G., Fernández Sevilla, J.M., Sánchez Pérez, J.A., Molina Grima, E., Chisti, Y., 2001. Airlift driven external-loop tubular photobioreactors for outdoor production of microalgae: assessment of design and performance. Chem. Eng. Sci. 56, 2721–2732.

Aiba, S., 1982. Growth kinetics of photosynthetic microorganisms. Adv. Biochem. Eng. 23, 85–156.

Alfano, O.M., Romero, R.L., Cassano, A.E., 1986. Radiation field modelling in photoreactors. I. Homogeneous media. Chem. Eng. Sci. 41, 421–444.

Camacho Rubio, F., Acién Fernández, F.G., Sánchez Pérez, J.A., García Camacho, F., Molina Grima, E., 1999. Prediction of dissolved oxygen and carbon dioxide concentration profiles in tubular photobioreactors for microalgal culture. Biotechnol. Bioeng. 62, 71–86.

Carlozzi, P., Torzillo, G., 1996. Productivity of *Spirulina* in a strongly curved outdoor tubular photobioreactor. Appl. Microbiol. Biotechnol. 45, 18–23.

Chisti, Y., 1989. Airlift Bioreactors. Elsevier, London.

Chisti, Y., Moo-Young, M., 1987. Airlift reactors: characteristics, applications and design considerations. Chem. Eng. Commun. 60, 195–242.

Chisti, Y., Moo-Young, M., 1993. Improve the performance of airlift reactors. Chem. Eng. Prog. 89 (6), 38–45.

Chisti, Y., 1999a. Shear sensitivity. In: Flickinger, M.C., Drew, S.W. (Eds.), Encyclopedia of Bioprocess Technology: Fermentation, Biocatalysis and Bioseparation, vol. 5. Wiley, New York, pp. 2379–2406.

Chisti, Y., 1999b. Mass transfer. In: Flickinger, M.C., Drew, S.W. (Eds.), Encyclopedia of Bioprocess Technology: Fermentation, Biocatalysis and Bioseparation, vol. 3. Wiley, New York, pp. 1607–1640.

Contreras Gómez, A., García Camacho, F., Molina Grima, E., Merchuk, J.C., 1998. Interaction between CO_2-mass transfer, light availability, and hydrodynamic stress in the growth of *Phaeodactylum tricornutum* in a concentric tube airlift photobioreactor. Biotechnol. Bioeng. 60, 317–325.

Laws, E.A., Satoru, T., Hirata, J., Pang, L., 1987. Optimization of microalgae production in a shallow outdoor flume. Biotechnol. Bioeng. 32, 140–147.

Mann, J.E., Myers, J., 1968. On pigments, growth and photosynthesis of *Phaeodactylum tricornutum*. J. Phycol. 4, 349–355.

Mirón, A.S., Gómez, A.C., Camacho, F.G., Grima, E.M., Chisti, Y., 1999. Comparative evaluation of compact photobioreactors for large-scale monoculture of microalgae. J. Biotechnol. 70, 249–270.

Molina Grima, E., 1999. Microalgae, mass culture methods. In: Flickinger, M.C., Drew, S.W. (Eds.), Encyclopedia of Bioprocess Technology: Fermentation, Biocatalysis and Bioseparation, vol. 3. Wiley, New York, pp. 1753–1769.

Molina Grima, E., García Camacho, F., Sánchez Pérez, J.A., Fernández Sevilla, J.M., Acién Fernández, F.G., Contreras Gómez, A., 1994a. A mathematical model of microalgal growth in light limited chemostat culture. J. Chem. Tech. Biotechnol. 61, 167–173.

Molina Grima, E., García Camacho, F., Sánchez Pérez, J.A., Urda Cardona, J., Acién Fernández, F.G., Fernández Sevilla, J.M., 1994b. Outdoor chemostat culture of *Phaeodactylum tricornutum* UTEX 640 in a tubular photobioreactor for the production of eicosapentaenoic acid. Biotechnol. Appl. Biochem. 20, 279–290.

Molina Grima, E., Acién Fernández, F.G., García Camacho, F., Chisti, Y., 1999. Photobioreactors: light regime, mass transfer, and scale up. J. Biotechnol. 70, 231–248.

Molina Grima, E., Acién Fernández, F.G., García Camacho, F., Camacho Rubio, F., Chisti, Y., 2001. Scale-up of tubular photobioreactors. J. Appl. Phycol. 12, 355–368.

Pirt, S.L., Lee, Y.K., Walach, M.R., Pirt, M.W., Balyuzi, H.H., Bazin, M.J., 1983. A tubular bioreactor for photosynthetic production of biomass from carbon dioxide: design and performance. J. Chem. Tech. Biotechnol. 33B, 35–58.

Qiang, H., Richmond, A., 1994. Optimizing the population density in *Isochrysis galbana* grown outdoor in a glass column photobioreactor. J. Appl. Phycol. 6, 391–396.

Richmond, A., Vonshak, A., 1978. *Spirulina* culture in Israel. Arch. Hydrobiol. Beih. Engebn. Limnol. 11, 274–280.

Terry, K.L., 1986. Photosynthesis in modulated light: quantitative dependence of photosynthetic enhancement on flashing rate. Biotechnol. Bioeng. 28, 988–995.

Torzillo, G., Carlozzi, P., Pushparaj, B., Montaini, E., Mat-

erassi, R., 1993. A two plane tubular photobioreactor for outdoor culture of *Spirulina*. Biotechnol. Bioeng. 42, 891–898.

Tredici, M.R., 1999. Bioreactors, photo. In: Flickinger, M.C., Drew, S.W. (Eds.), Encyclopedia of Bioprocess Technology: Fermentation, Biocatalysis and Bioseparation, vol. 1. Wiley, New York, pp. 395–419.

Tredici, M.R., Zitelli, G.C., Biagiolini, S., 1992. Influence of turbulence and areal density on the productivity of *Spirulina platensis* grown outdoor in a vertical alveolar panel. In: First European Workshop on Microalgal Biotechnology, Bergholz-Rehbrucke, pp. 58–60.

Vandanjon, L., Rossignol, N., Jaouen, P., Roberts, J.M., Quéméneur, F., 1999. Effects of shear on two microalgae species. Contribution of pumps and valves in tangential flow filtration systems. Biotechnol. Bioeng. 63, 1–9.

Vonshak, A., Cohen, Z., Richmond, A., 1985. The feasibility of mass cultivation of *Porphyridium*. Biomass 8, 13–25.

Weissman, J.C., Goebel, R.P., Benemann, J.R., 1988. Photobioreactor design: mixing, carbon utilization, and oxygen accumulation. Biotechnol. Bioeng. 31, 336–344.

Yongmanitchai, W., Ward, O., 1991. Growth of and omega-3 fatty acid production by *Phaeodactylum tricornutum* under different culture conditions. Appl. Environ. Microbiol. 2, 419–425.

Zuber, N., Findlay, J.A., 1965. Average volumetric concentration in two phase flow systems. J. Heat Trans. Trans. ASME 453, 457.